

REAL-TIME BEAM DETECTION AND TRACKING FROM PINHOLE IMAGING SYSTEM BASED ON MACHINE LEARNING

A. A. Nosych, U. Iriso, ALBA Synchrotron, Barcelona, Spain

Abstract

At ALBA Synchrotron each of the two in-air pinhole imaging systems is able to see several beam spots at once due to specific pinhole grid with 3x3 holes placed in the path of the X-ray fan. Each beam image has its own properties, such as source pinhole aperture size, its Point Spread Function (PSF) and copper filter thickness, all of which impact the electron beam size calculation. Until now, these parameters were applied manually to the pinhole device servers for numerical image analysis, so this semi-manual beam size calculator is subject to frequent adjustments and human monitoring.

This study looks at feasibility of training and pointing an Artificial Neural Network (ANN) at image stream coming from pinhole cameras in real time, track all detected beam spots and analyze them, with the end goal to automate the whole pinhole beam image processing.

INTRODUCTION

The ALBA Synchrotron is a 3 GeV third-gen light source located in Cerdanyola del Vallès (Barcelona, Spain). Currently it has 10 operational beamlines, comprising soft and hard X-rays that perform research in fields like material science, condensed matter, nanotechnology, biology and others. The facility provides more than 6000 hours of beam time per year and is available for the academic and the industrial sector, serving several thousand researchers every year.

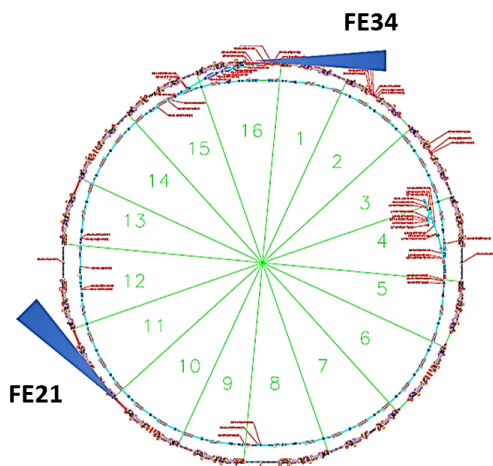


Figure 1: ALBA storage ring layout, and location of both in-air X-ray pinholes in sectors 1 and 11.

Measuring transverse size and emittance [1] of the electron beam at any moment of time is essential to control the machine performance. This measurement is carried out by two in-air X-ray pinhole cameras [2], whose location is shown in Fig. 1 and components laid out in Fig. 2.

Apart from emittance and beam size, the pinholes inevitably monitor beam position and stability. As the simple optics principle of a pinhole, it takes the synchrotron radiation coming from a bending magnet to obtain a magnified transverse image of an electron beam, which is analysed to infer the horizontal and vertical (H and V) electron beam size. Any movement of beam orbit will immediately be seen in the pinholes, and any problematic beam will be observed as blurred, out of shape, or different in size than usual.

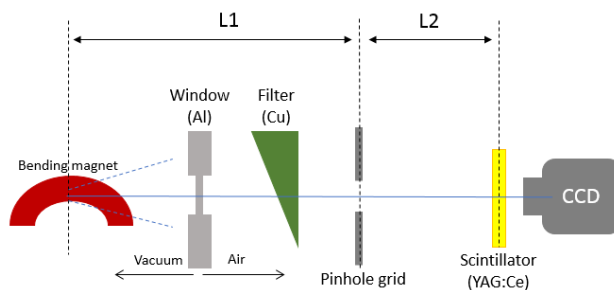


Figure 2: Component schematics of ALBA pinhole system (not to scale).

Since its commissioning in 2011 the storage ring has been operating with only one pinhole located at front-end 34 (FE34) [3], but in 2020 a second pinhole at front-end 21 (FE21) was installed for redundancy. It brings a few improvements with respect to FE34, the main of which is higher magnification. See Table 1 for a list of other differences.

Table 1: ALBA's Pinholes Compared

	FE21	FE34
L1	4.111 m	5.936 m
L2	15.357 m	13.828 m
Magnification	3.76	2.31
Visible beam spots	2	6
Al window thickness	1.5 mm	1 mm
Beam size at source	56, 26 μm	53, 23 μm

Both ALBA's X-ray pinhole lines are similar and consist of a chain of elements shown in Fig. 2. This type of pinhole system has previously been described in greater detail [2–4], so we will not focus on its functionality here. The elements important for this work are the copper wedge filter (an X-ray attenuator) and the pinhole grid itself.

The pinhole grid is motorized and has 4 degrees of freedom (lateral, vertical, rotational and pitch). It consists of apertures made by horizontal and vertical tungsten bars (Fig. 3): in total there are 9 rectangular holes of different size, with 3 squared. FE21 and FE34 share the 50x50 and 10x10 μm

Content from this work may be used under the terms of the CC BY 3.0 licence (© 2021). Any distribution of this work must maintain attribution to the author(s), title of the work, publisher, and DOI

hole sizes, while FE34 also has the 100×100 μm and FE21 the 5×5 μm. The values 100, 50, 10 and 5 μm are theoretical: the true apertures were measured in the lab with optical microscopy and diffraction methods and are slightly larger.

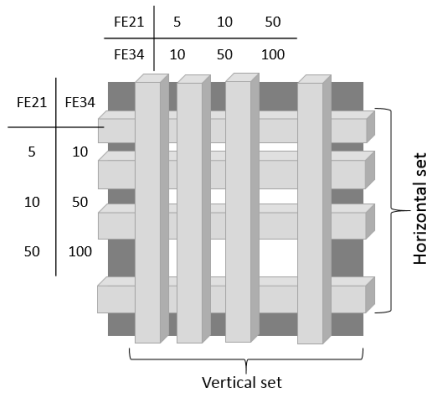


Figure 3: Schematic of a pinhole grid made of 1 mm thick tungsten bars crossing into 9 apertures of different sizes.

PINHOLE IMAGE PROCESSING

The frames stream at 3 Hz rate from both pinhole CCD. For simplicity and speed the frames are cropped around a region of interest (ROI), which is manually fixed to tell the control system where to look, Fig. 4. Device server then does 1D projection Gaussian fits on the fly for beam size estimation. This is sufficient during stable operation of the machine for users. We usually select the ROI around the 10×10 μm pinhole due to its smallest PSF contribution (more on this below). This is reliable and quick, provided the beam does not move.

If the beam or the pinhole grid motors move for some reason, the ROI must be adjusted manually. Moreover, for machine studies and optimization a 2D Gaussian fit must be performed frequently and manually. Here is the part where using machine learning and ANN can come in handy and bring pinhole image analysis on a whole another level.

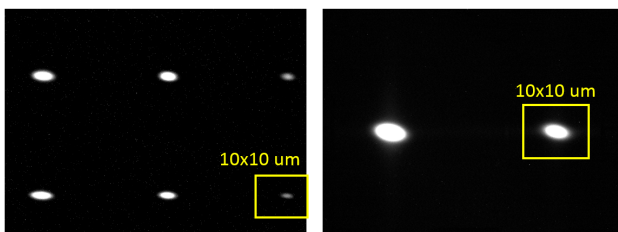


Figure 4: Complete images seen by both pinhole CCDs (FE34 left and FE21 right) while in operation with beam.

Due to grid structure of the pinhole sets, both cameras are able to “see” up to 8 beam spots combined, with FE21 viewing less spots (only 2) due to shorter distances between mechanical elements and larger magnification. So what if we were to look and analyse all of them at once? This becomes

a practical *computer vision* application of machine learning algorithms for beam diagnostics!

For fully automated and reliable beam size and emittance monitoring in 2D a computer vision model can be trained to look at the stream of CCD frames, detect all beam spots, and pass their coordinates to mathematical analysis routine. However, one thing must be taken care of.

PSF Calculation

The pinhole image is affected by the system PSF, which is the beam size measured at the camera screen corresponding to a point-like electron beam. Among other characteristics, the PSF strongly depends on the pinhole aperture size and radiation wavelength λ . Here, λ is defined by the Al window thickness (fixed) and the copper filter attenuation (variable).

To emulate a PSF a unit-size electron beam is defined. It is also called a “zero emittance beam” and it combines blurring and diffraction effects [3, 4]:

$$\sigma_{\text{PSF}} = \sqrt{\sigma_{\text{blur}}^2 + \sigma_{\text{diff}}^2 + \sigma_{\text{scr}}^2}, \quad (1)$$

where σ_{diff} is Fraunhofer diffraction

$$\sigma_{\text{diff}} = \frac{\sqrt{12} \lambda L_2}{4\pi w}, \quad (2)$$

σ_{blur} is blurring due to the finite size of the pinhole

$$\sigma_{\text{blur}} = \frac{w(L_1 + L_2)}{\sqrt{12}L_1}, \quad (3)$$

w is pinhole width or height, and σ_{scr} is the CCD pixel size.

Taking all of this into account, the measured size of a beam spot σ_{YAG} will be larger than the true electron beam size σ_b , due to its PSF:

$$\sigma_{\text{YAG}}^2 = (M\sigma_b)^2 + (\sigma_{\text{PSF}})^2, \quad (4)$$

where $M = \frac{L_2}{L_1}$ is the pinhole magnification.

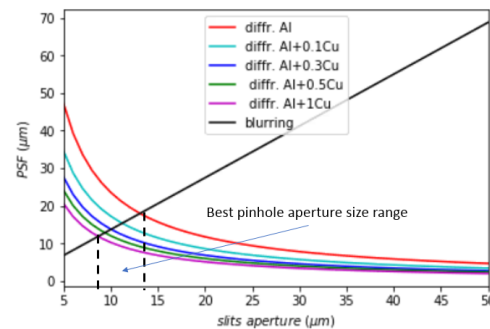


Figure 5: Simulated blurring and diffraction contributions to PSF as functions of pinhole aperture w and Cu thickness. Apertures with sizes 50 μm and larger must be used with care, because they can actually enlarge the beam measurement.

It is always best to build and set up the system mechanically such that PSF is minimal from the start, before any

Content from this work may be used under the terms of the CC BY 3.0 licence (© 2021). Any distribution of this work must maintain attribution to the author(s), title of the work, publisher, and DOI

numerical analysis. The blurring contribution is independent of the pinhole aperture size in H and V, so by combining blurring with diffraction, Fig. 5, we can estimate analytically the size of pinhole apertures with smallest PSF: 9-14 μm . This is why we prefer to work with pinholes of apertures of 10x10 μm , and have other aperture sizes for cross-checks.

Accurate characterization of the pinhole PSF is essential for the transverse beam size and emittance calculation. The PSF can be calculated by three different methods: analytically (Eqs. (1-3)), experimentally and by numerical simulations. Until recently, the PSF has only been calculated analytically for pinhole in FE34 [3]. Now with the addition of another pinhole, it became necessary to compare the analytical calculations with the experimental results and simulations.

We have concluded that three methods of PSF calculation are consistent [4], and mapped PSF values against true pinhole apertures and Cu thickness for each pinhole:

$$\text{PSF}(t, w) = \begin{cases} \text{PSF}_{\text{Al}}, & \text{if } t < 0.1 \mu\text{m} \\ \frac{A(w)}{t} + B(w)t + C(w), & \text{if } t \geq 0.1 \mu\text{m} \end{cases} \quad (5)$$

where PSF_{Al} is PSF of Al window itself without the filter, and t is copper thickness corresponding to the beam spot location on the YAG (see next Section). The fit coefficients A, B, C are different for each w and front-end.

Using this parametric function Eq. (5) we can calculate PSF for any pinhole aperture and Cu filter position, once we know them, and correct our beam size measurements in Eq. (4).

Copper Filter

The copper filter is a wedge-shaped block (a tall right trapezoid) in front of a pinhole grid, Fig. 2. By sliding in/out the block, we are choosing different Cu thickness, and hence control the flux (more Cu – harder X-rays). It also plays several very important roles: 1) reduce heat load on the pinhole grid and renders unnecessary any additional cooling, 2) help avoid CCD image saturation, and 3) produce a monochromatic light to avoid possible chromatic effects.

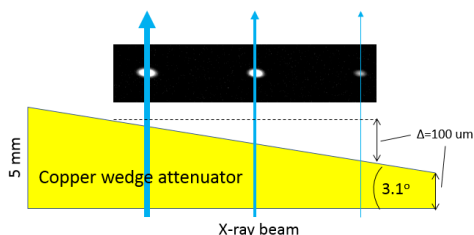


Figure 6: Relation between the Cu filter position and beam spots on the CCD image: each spot receives X-ray flux passed through different Cu thickness (not to scale).

Both the filter and the pinhole grid can move laterally independently of each other. Figure 6 demonstrates that each beam spot receives a different amount of flux depending

on mechanical positions of the pinhole grid and Cu filter, so each spot requires a slightly different PSF for correction. The difference in copper thickness between extreme horizontal pixels of the image is around 100 μm : comparable to minimum thickness of the filter itself, so it is not negligible.

Since positions of the filter and pinhole grid motors are known, they can be mapped against each other and against the horizontal pixel coordinates of the fixed CCD image (vertical is irrelevant here) to keep track of the pinhole apertures and Cu filter thickness in view of the CCD. This way we can relate any beam spot centroid with w and t .

Now, using w and t for the PSF input, we can move on to actual ANN training and image analysis.

COMPUTER VISION FOR BEAM DIAGNOSTICS

This chapter is is work in progress. It talks about intermediate results obtained after recent pinhole upgrades at ALBA. No other computer vision applications have been developed for Beam Diagnostics at the time of this work.

In order to have automated beam tracking from image stream the software needs to recognise the beam spots, whether Gaussian shapes or any general blobs distinct from the background. It requires supervised learning to classify objects (e.g. beam spots) and must be trained on a set of prepared samples that contain necessary classifiers (i.e. known objects with names). One of the appropriate algorithms at the time of this study appeared to be YOLOv3 [5] with TensorFlow v2.4 [6] backend.

YOLO stands for *You Only Look Once* and it is a handy real-time object detection system based on convolutional ANN which looks at the whole image at once and predicts bounding boxes with classifiers. Its main advantages are speed and model size: a well-trained model is able to detect multiple objects from a live video stream.

For our purposes we train a YOLO model on a single classifier “beam”, since we don’t have other significant objects seen by pinhole CCDs.

In machine learning each model is a hypothesis that predicts a value given a set of input values. The model has a set of weights which are tuned based on a set of training data. A loss function is used to determine how far the predicted values deviate from the actual values in the training data. Training a model is about tuning the model weights by the algorithm to make the loss minimum.

For training a model from scratch a dataset of 300 random 2D Gaussian distributions that resemble beam spots (100x100 px images) is generated along with annotations. Another 50 images are added as a control dataset.

Already with this minimal recommended dataset size, training a working model is feasible without paralleling: on a 3 GHz desktop PC a first “good” model already shows up after 20 learning epochs, with each epoch lasting under 2 hours of CPU time.

Figure 7 shows loss value evolution during iterative training and an average number of detected “beam” objects (6 is

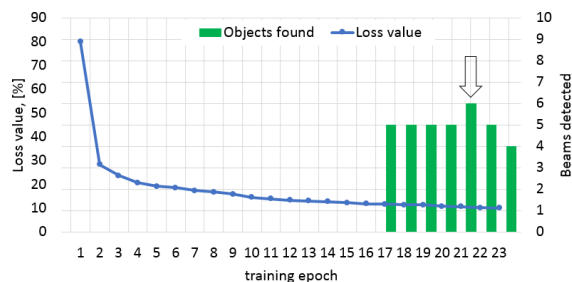


Figure 7: Loss value evolution during iterative YOLO model training vs. max beam objects found by several last models. The "smartest" model of the set is highlighted.

the maximum, Fig. 4). Figure 8 shows the result of using the "smartest" model to detect "beams" on a single CCD frame.

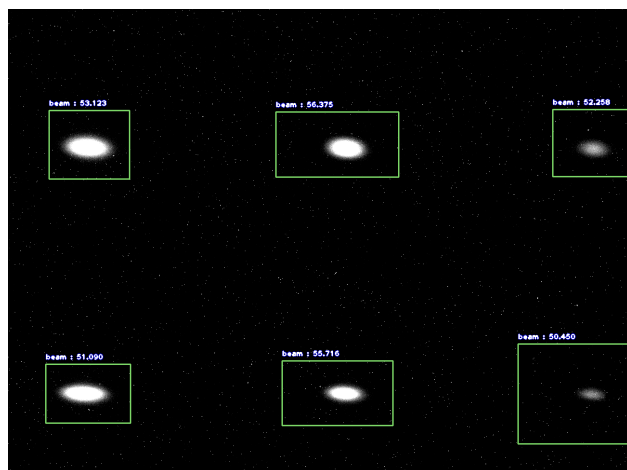


Figure 8: A single pinhole CCD frame with 6 beam spots detected by a trained YOLO model.

Automatic detection of beam spots is half of the desired functionality. Another half is the efficient and robust automatic numerical analysis of those spots. Using dynamic PSF calculator for every detected beam spot we fit them with the 2D Gaussian function and apply corrections: remove PSF contribution, magnification, and finally scale px to mm to get accurate electron beam size, emittance and coupling.

Figure 9 demonstrates very successful results of using the developed system to track beam coupling changes. Here the ANN is looking at the same beam spot (FE34 top row and FE21 bottom row) while the coupling factor changes from small (0.15%), to nominal (0.6%) to high (1.4%). The images are processed at 0.5 fps on a laptop and all output values (beam size, tilt angle, coupling, etc.) are accurate and expected, similar to the ones obtained manually before.

CONCLUSION

We have built a working and accurate real-time beam tracking and image analysis software system based on machine learning. The developed system works at the speed of around 0.5-1 fps on a standard PC, which is already feasible for some machine studies in real-time.

The detection system still has to be studied to deal with several important challenges, e.g. improving the detection score,

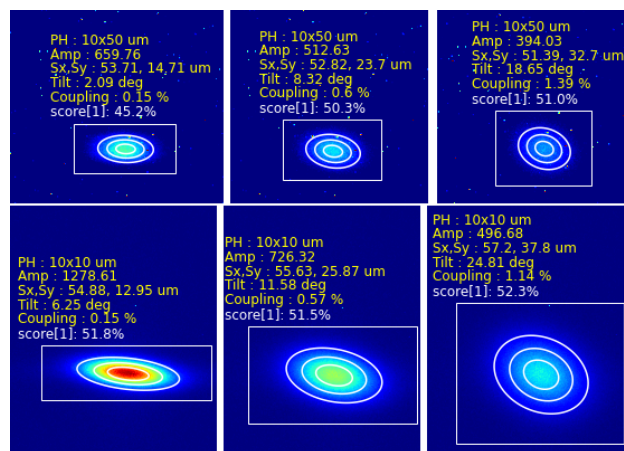


Figure 9: Tracking the same beam spot in both pinholes while changing the coupling factor along the storage ring.

and speed up to at least 3 Hz. It is also clear, that a "smarter" model can be trained, and it requires better learning data, longer training time, and powerful parallel hardware to learn (CPU->GPU->HPC).

Moreover, the reality and variety of operational conditions, beam experiments and anomalies show that beam spots on the YAG screen can vary a lot in shape, size, position and brightness. Training a model only on artificial 2D Gaussians may not produce clever enough image recognition model.

Alternatively, the model can be reinforced with a real image dataset (>300 samples), but the task of annotating every beam object on hundreds of images is massive, must be done by hand (e.g. with **LabelImg** python tool). However, it may be worth the effort in pursuit of full automation.

ACKNOWLEDGEMENTS

The authors would like to express their thanks to Ingrid Mases Solé and Alba Cazorla for meticulousness and persistence in tackling PSF studies, and Dominique Heinis for priceless help on ANNs.

REFERENCES

- [1] A. Wu Chao, M. Tigner, *Handbook of Accelerator Physics and Engineering*. World Scientific. 1998.
- [2] V. Suller, "An X-ray Pinhole Camera Design for the ALBA Synchrotron Light Source", April 2005.
- [3] U. Iriso, "Beam Size and Emittance Measurements using the ALBA Pinhole", Barcelona, Spain, ALBA Internal Note AAD-SR-DI-PINH-01, June 2011.
- [4] Ingrid Mases Solé, "Characterization of the PSF for the X-ray pinhole cameras at ALBA Synchrotron", Treball de Fi de Grau, Facultat de Física, Universitat de Barcelona, 2020.
- [5] Redmon Joseph, Farhadi Ali, "YOLOv3: An Incremental Improvement", arXiv, 2018. <https://pjreddie.com/darknet/yolo>
- [6] Martín Abadi *et al.*, "TensorFlow: Large-Scale Machine Learning on Heterogeneous Systems", 2015. <https://www.tensorflow.org>